FOCAD loss impacts microtubule assembly, G2/M progression and patient survival in astrocytic gliomas

Brand, Frank ; Förster, Alisa ; Christians, Anne ; Bucher, Martin ; Thomé, Carina M ; Raab, Marc S ; Westphal, Manfred ; Pietsch, Torsten ; von Deimling, Andreas ; Reifenberger, Guido ; Claus, Peter ; Hentschel, Bettina ; Weller, Michael ; Weber, Ruthild G

Abstract: In search of novel genes associated with glioma pathogenesis, we have previously shown frequent deletions of the KIAA1797/FOCAD gene in malignant gliomas, and a tumor suppressor function of the encoded focadhesin impacting proliferation and migration of glioma cells in vitro and in vivo. Here, we examined an association of reduced FOCAD gene copy number with overall survival of patients with astrocytic gliomas, and addressed the molecular mechanisms that govern the suppressive effect of focadhesin on glioma growth. FOCAD loss was associated with inferior outcome in patients with isocitrate dehydrogenase 1 or 2 (IDH)-mutant astrocytic gliomas of WHO grades II-IV. Multivariate analysis considering age at diagnosis as well as IDH mutation, MGMT promoter methylation, and CDKN2A/B homozygous deletion status confirmed reduced FOCAD gene copy number as a prognostic factor for overall survival. Using a yeast two-hybrid screen and pull-down assays, tubulin beta-6 and other tubulin family members were identified as novel focadhesin-interacting partners. Tubulins and focadhesin co-localized to centrosomes where focadhesin was enriched in proximity to centrioles. Focadhesin was recruited to microtubules via its interaction partner SLAIN motif family member 2 and reduced microtubule assembly rates, possibly explaining the focadhesin-dependent decrease in cell migration. During the cell cycle, focadhesin levels peaked in G2/M phase and influenced time-dependent G2/M progression potentially via polo like kinase 1 phosphorylation, providing a possible explanation for focadhesin-dependent cell growth reduction. We conclude that FOCAD loss may promote biological aggressiveness and worsen clinical outcome of diffuse astrocytic gliomas by enhancing microtubule assembly and accelerating G2/M phase progression.

DOI: https://doi.org/10.1007/s00401-019-02067-z

FOCAD loss impacts microtubule assembly, G2/M progression and patient survival in astrocytic gliomas

Frank Brand[1], Alisa Förster[1], Anne Christians[1], Martin Bucher[1], Carina M. Thomé[2], Marc S. Raab[3,4], Manfred Westphal[5*], Torsten Pietsch[6*], Andreas von Deimling[7,8*], Guido Reifenberger[9,10*], Peter Claus[11], Bettina Hentschel[12*], Michael Weller[13*], Ruthild G. Weber[1]

[1]Department of Human Genetics, Hannover Medical School, Hannover, Germany
[2]Neurology Clinic and National Center for Tumor Diseases, Clinical Cooperation Unit Neurooncology, German Cancer Research Center (DKFZ), Heidelberg, Germany
[3]Department of Internal Medicine V, Hematology, Oncology and Rheumatology, University of Heidelberg, Heidelberg, Germany
[4]Clinical Cooperation Unit Molecular Hematology / Oncology, German Cancer Research Center (DKFZ), Heidelberg, Germany
[5]Department of Neurosurgery, University Medical Center Hamburg-Eppendorf, Hamburg Germany
[6]Department of Neuropathology, University of Bonn Medical School, Bonn, Germany
[7]Department of Neuropathology, Institute of Pathology, University Hospital Heidelberg, Heidelberg, Germany
[8]Clinical Cooperation Unit Neuropathology, German Consortium for Translational Cancer Research (DKTK), German Cancer Research Center (DKFZ), Heidelberg, Germany
[9]Department of Neuropathology, Heinrich-Heine-University, Düsseldorf, Germany
[10]German Cancer Consortium (DKTK), Partner Site Essen/Düsseldorf and German Cancer Research Center (DKFZ), Heidelberg, Germany
[11]Department of Neuroanatomy and Cell Biology, Hannover Medical School, Hannover, Germany, and Center for Systems Neuroscience (ZSN), Hannover, Germany
[12]Institute for Medical Informatics, Statistics and Epidemiology, University of Leipzig, Leipzig, Germany
[13]Department of Neurology, University Hospital and University of Zurich, Zurich, Switzerland

*These authors represent the German Glioma Network

Correspondence to: Ruthild G. Weber, M.D., Department of Human Genetics OE 6300, Hannover Medical School, Carl-Neuberg-Str. 1, D-30625 Hannover, Germany, Phone: +49 511 5327751, Fax: +49 511 53218520, E-mail: weber.ruthild@mh-hannover.de

Short running title: *FOCAD* loss in astrocytic gliomas

Abstract

In search of novel genes associated with glioma pathogenesis, we have previously shown frequent deletions of the *KIAA1797/FOCAD* gene in malignant gliomas, and a tumor suppressor function of the encoded focadhesin impacting proliferation and migration of glioma cells *in vitro* and *in vivo*. Here, we examined an association of diminished *FOCAD* copy number with overall survival of patients with astrocytic gliomas, and addressed the molecular mechanisms that govern the suppressive effect of focadhesin on glioma growth. *FOCAD* loss was associated with inferior outcome in patients with isocitrate dehydrogenase 1 or 2 (IDH)-mutant astrocytic gliomas of WHO grades II-IV. Multivariate analysis considering age at diagnosis as well as IDH mutation, *MGMT* promoter methylation, and *CDKN2A/B* homozygous deletion status confirmed *FOCAD* loss as a prognostic factor for overall survival. Using a yeast two-hybrid screen and pull-down assays, tubulin beta-6 and other tubulin family members were identified as novel focadhesin-interacting partners. Tubulins and focadhesin co-localized to centrosomes where focadhesin was enriched in proximity to centrioles. Focadhesin was recruited to microtubules via its interaction partner SLAIN motif family member 2 and reduced microtubule assembly rates, possibly explaining the focadhesin-dependent decrease in cell migration. During the cell cycle, focadhesin levels peaked in G2/M phase and influenced time-dependent G2/M progression potentially via polo like kinase 1 phosphorylation, providing a possible explanation for focadhesin-dependent cell growth reduction. We conclude that *FOCAD* loss may promote biological aggressiveness and worsen clinical outcome of diffuse astrocytic gliomas by enhancing microtubule assembly and accelerating G2/M phase progression.

Keywords: FOCAD; astrocytic glioma; prognosis; centrosome; microtubules; cell cycle

Introduction

Diffuse astrocytic gliomas are diffusely infiltrating brain tumors classified by the World Health Organization (WHO) as diffuse astrocytoma (WHO grade II), anaplastic astrocytoma (WHO grade III), and glioblastoma (WHO grade IV) based on histologic characteristics [27]. In addition, molecular genetic parameters are used to more precisely define these tumor categories by assessing the presence or absence of mutations in the isocitrate dehydrogenase (IDH) genes *IDH1* and *IDH2* [27]. Furthermore, the absence of a combined loss (codeletion) of chromosomal arms 1p and 19q distinguishes IDH-mutant diffuse astrocytic gliomas from IDH-mutant and 1p/19q-codeleted oligodendroglial tumors [27, 34]. IDH mutation and 1p/19q codeletion status are, therefore, highly relevant diagnostic markers that are also closely linked to outcome of patients with diffuse gliomas [5, 46]. Consequently, an integrated histomolecular classification of diffuse gliomas must be used in current attempts at identifying new biomarkers that may prognostically stratify diffuse glioma patients and guide tumor grading. The identification of novel molecular alterations associated with patient outcome and the characterization of the pathomechanisms involved are also required for the design of risk-stratified treatment strategies for the different glioma entities.

Chromosomal aberrations implicated in the progression and clinical aggressiveness of diffuse astrocytic gliomas are deletions of the entire chromosomal arm 9p or parts thereof (e.g. [5, 46]). These deletions are thought to preferentially target the cyclin dependent kinase inhibitor 2A and 2B (*CDKN2A/B*) genes at 9p21.3 [1, 6, 39]. In addition to *CDKN2A/B*, however, the 9p deletions commonly encompass several other genes potentially playing important roles in driving glioma progression [36]. We have previously shown that the *KIAA1797/FOCAD* gene located in close proximity to *CDKN2A/B* in the same chromosomal subband is also frequently deleted, and that the encoded focadhesin (FOCAD) functions as a tumor suppressor in glioblastoma [4]. *FOCAD* re-expression in glioblastoma cells with homozygous *FOCAD* deletion inhibited cell migration and invasion as well as proliferation *in vitro* and *in vivo* [4]. *FOCAD* deletions have also been implicated in the pathogenesis of other tumor entities, e.g. breast cancer, where somatic and germline deletions of the *FOCAD* gene

were described in sporadic cases without mutation in the BRCA1 DNA repair associated (*BRCA1*) gene [24, 29]. In addition, heterozygous microdeletions or truncating mutations of the *FOCAD* gene have been detected in the germline of colorectal cancer and adenomatous polyposis patients [17, 43, 48], corroborating a role for *FOCAD* haploinsufficiency or inactivation in the predisposition for and growth of various cancer entities.

This study aimed at gaining further insights into the relevance of diminished *FOCAD* copy number for the pathogenesis of diffuse astrocytic gliomas and the pathomechanisms involved. We explored the frequency and prognostic value of diminished *FOCAD* copy number in a prospective cohort of patients with astrocytic gliomas of WHO grades II to IV. Since little is known about the cellular localization and function of FOCAD, we determined FOCAD binding partners in a yeast two-hybrid screen, visualized the cellular site of their interaction, and performed functional and biochemical assays to characterize how FOCAD functions as a tumor suppressor. We report that tubulin-binding FOCAD localizes to centrosomes impacting microtubule assembly and cell cycle progression in the G2/M phase, and that *FOCAD* loss is a prognostic marker for overall survival (OS) in patients with IDH-mutant astrocytic gliomas.

Materials and methods

Patients and tumors

The German Glioma Network (GGN, www.gliomnetzwerk.de) is a prospective, non-interventional cohort study involving eight clinical centers at German university hospitals, which was supported by the German Cancer Aid from 2004 to 2012. All patients gave written informed consent for participation in the GGN and its translational research projects. All tumors were subjected to central pathology review (T.P.) and initially classified according to the WHO classification of tumors of the central nervous system of 2007 [26]. For this study, all tumors were reclassified according to the revised 4th edition of the WHO classification 2016 [27] based on *IDH1* and *IDH2* (IDH) mutation status previously determined by direct

sequencing of tumor DNA and 1p/19q codeletion status [33, 46]. Data on 1p/19q codeletion as well as *FOCAD* and *CDKN2A/B* copy number were retrieved from previously reported array-based comparative genomic hybridization (CGH) results using the diagnostic cut-offs <-0.3 >-1 to score loss and ≤-1 to score homozygous deletion; O^6-methylguanine-DNA-methyltransferase (*MGMT*) promoter methylation status had been determined by methylation-specific PCR [33, 46]. In the present study, only gliomas without 1p/19q-codeletion were included, thus restricting the prognostic association studies to patients with IDH-wildtype or IDH-mutant diffuse astrocytic gliomas. The clinical and pathologic characteristics of the study cohort are summarized in Table 1. The median follow-up was 8.5 years (range: 0.6-17.7 years), with 85 deaths (63.9%) and 48 patients (36.1%) alive at last follow-up.

Cells, transfection, and treatments

HeLa S3 cells, HEK293T cells, human glioblastoma cell lines LN-18 (*FOCAD*$^{-/-}$) and U-87MG (*FOCAD*$^{-/-}$) with *FOCAD* homozygous deletions, LN-229 (*FOCAD*$^{+/+}$) with balanced *FOCAD* and *CDKN2A/B* status according to high-resolution array-based CGH analysis [4] were cultured as described in Supplementary material online resource. Human astrocytes and culture medium were purchased from ScienCell (ScienCell Research Laboratories, Carlsbad, CA, USA). All cells were transfected using Lipofectamine 3000 (Thermo Fisher Scientific, Waltham, MA, USA). For cell synchronization at G1/S and M phase, double thymidine block (Sigma-Aldrich, St. Louis, MO, USA; 2 mM, 16 h each) or nocodazole (Sigma-Aldrich; 100 ng/ml, 16 h) were applied. To assess protein stability, cells were treated with biosynthesis inhibitor cycloheximide (Sigma-Aldrich; 20 µg/ml), 26S proteasome inhibitors bortezomib (Sigma-Aldrich; 100 nM) or MG132 (Sigma-Aldrich; 10 µM).

Plasmids

The primers used to generate constructs are given in Supplementary material online resource. To generate the FOCAD yeast two-hybrid bait construct, the full-length open

reading frame (ORF) of *FOCAD* was amplified from cDNA derived from human astrocytes and cloned into the multiple cloning site of the bait vector pEG202 (MoBiTec, Göttingen, Germany), resulting in pEG202-FOCAD. To generate a construct expressing N-terminal GFP-tagged FOCAD, the *FOCAD* ORF was amplified from pEG202-FOCAD and subcloned into the pEGFP-C1 expression vector (Takara Bio) (=GFP-FOCAD). To generate a lentivector construct expressing C-terminal GFP-tagged FOCAD, the *FOCAD-GFP* cDNA was cloned 3' of a cytomegalovirus (CMV) promoter resulting in rrl-cPPT-CMV-FOCAD-GFP-WPRE (=FOCAD-GFP). The lentivector plasmid was used for transient transfection. The pcDNA3.1 expression vector coding for untagged FOCAD was described previously [4]. The ORFs of *TUBA1A*, *TUBB3*, *TUBB6*, *TUBG1,* and *SLAIN2* were amplified from Human Multiple Tissue cDNA Panel I (#636747, LOT1212243A; Takara Bio, Kusatsu, Japan) and subcloned into the pcDNA3.1-Myc (Thermo Fisher Scientific) or the pTagRFP (RFP) expression vector (Evrogen, Moscow, Russia). All constructs were verified by restriction enzyme digest and direct sequencing. The human full-length HSP90AB1 cDNA in a pcDNA3.1/GS expression vector was purchased from Thermo Fisher Scientific/Invitrogen.

FOCAD bait yeast two-hybrid screen with a human brain cDNA prey library

A yeast two-hybrid screen was performed according to the manufacturer's protocol (MoBiTec). In brief, the pEG202-FOCAD bait vector coding for the DNA-binding domain of LexA fused to FOCAD was used together with prey vectors pJG4-5 comprising a human fetal brain cDNA library (Origene Technologies Inc, Rockville, MD, USA) under the control of the inducible GAL1 promoter and as translation fusions with the B42 acidic activator. The plasmids were transformed into the *S. cerevisiae* strain EGY48 (*MAT*α, *trp1*, *his3, ura3, leu2::6 LexAop-LEU2*; MoBiTec). Positive yeast clones were identified by growth on synthetic defined (SD) medium supplemented with galactose (gal) and raffinose (raf) and lacking histidine, leucine, and tryptophan (SD(gal/raf)ΔHLT; all purchased from MoBiTec). False-positive clones, which grew on SD medium supplemented with glucose (SD(glu)ΔHLT), were not characterized further. The remaining prey-inserts were analyzed by direct DNA

sequencing of yeast colony-PCR products amplified using the primer pair 5'-ATA TCG AGG AGT GCA ATG CC-3' (forward) and 5'-GCC GAC AAC CTT GAT TG-3' (reverse). Reconstitution of bait and prey interaction was verified by retransformation of yeast cells following the lithium acetate method described in the yeast protocol handbook (Takara Bio). Comparable growth of yeast co-transformants was verified on SD(gal/raf)ΔHT medium (with leucine) required for plasmid selection.

Pull-down assays

Binding of FOCAD to HSP90AB1 was verified using 6xHis-tag-mediated pull down as detailed in Supplementary material online resource. Binding of FOCAD to tubulin isoforms was assayed using Myc-tag-mediated pull down. HEK293T cells were transiently co-transfected with constructs expressing N-terminal Myc-tagged TUBA1A, TUBB3, TUBB6 or TUBG1 and untagged FOCAD. At 24 h post transfection, cells were washed with ice-cold phosphate-buffered saline (PBS) and lysed for 30 min on ice in 1 ml of immunoprecipitation (IP) lysis buffer (20 mM Tris-HCl, pH 8.0), 50 mM sodium fluoride, 1 mM sodium orthovanadate, 1% Triton X-100, supplemented with protease and phosphatase inhibitors (Roche Diagnostics)). Cell lysates were incubated with 1 µg of anti-Myc antibody (sc-40; Santa Cruz Biotechnology, Dallas, TX, USA) by tumbling over night at 4°C. Protein G Sepharose beads (GE Healthcare, Little Chalfont, UK) were equilibrated in IP lysis buffer, blocked with 0.1% bovine serum albumin (BSA; Thermo Fisher Scientific) and incubated with the lysates for 4 h at 4°C. After five washing steps with IP lysis buffer, bound protein was eluted from the beads using Laemmli buffer (62.5 mM Tris-HCl, pH 6.8, 10% glycerol, 2% SDS, 5% 2-mercaptoethanol, 1 mM EDTA, 0.01% bromophenol blue), and detected by Western blot analysis.

Western blot analysis

After sodium dodecylsulfate-polyacrylamide gel electrophoresis and semidry electroblotting, polyvinylidene difluoride or nitrocellulose membranes (GE Healthcare) were blocked with 5%

fat-free milk powder dissolved in PBS with 0.05% Tween 20 (PBST). Primary antibodies given in Supplementary material online resource were diluted in 5% (w/v) BSA in PBST and used for immunodetection. After incubation over night at 4°C, membranes were exposed to the appropriate horseradish peroxidase-conjugated secondary antibody (Santa Cruz Biotechnology; dilution 1:3,000) in 5% fat-free milk powder dissolved in PBST for 90 min at room temperature, and developed using the Pierce SuperSignal West Femto or Dura Substrate detection kit (Thermo Fisher Scientific). Signals were acquired using the Fusion FX7 gel documentation system (Vilber, Collégien, France).

Generation of cell lines with stable GFP-tagged FOCAD expression or FOCAD knockdown

To generate stable expression of GFP-tagged FOCAD, LN-18 and U-87MG (both *FOCAD*$^{-/-}$) cells were transfected with pEGFP-C1 or pEGFP-C1-FOCAD (=GFP-FOCAD), and selected with 600 µg/ml geneticin (Thermo Fisher Scientific) for at least 14 days starting 48 h post transfection. GFP-positive cells were isolated at the Cell Sorting Core Facility of Hannover Medical School using a MoFlo™ XDP cell sorter (Beckman-Coulter, Brea, MA, USA). A stable FOCAD knockdown was generated in LN-229 (*FOCAD*$^{+/+}$) cells as described in Supplementary material online resource.

Immunofluorescence

Cells were seeded on collagen-coated coverslips and transiently transfected, if necessary. For the enrichment of mitotic cells, LN-18 and HEK293T cells were analyzed 10 h after release from second thymidine block. All cells were fixed with 2% paraformaldehyde in PHEM buffer (60 mM PIPES, 27 mM HEPES, 10 mM EGTA, 4 mM $MgSO_4$; adjusted to pH 7.0) followed by treatment with methanol for 20 min at -20°C. Primary antibodies are given in Supplementary material online resource. Secondary antibodies were conjugated to Alexa Fluor 488 or 568 (Thermo Fisher Scientific). DNA was counterstained with 4',6-diamidino-2-phenylindole (Sigma-Aldrich). Images were captured using a confocal (Leica DM IRB with a

TCS SP2 AOBS scan head, Leica Microsystems, Wetzler, Germany) or an epifluorescence microscope (Leica DM RXA2) equipped with a cooled charge-coupled device camera (SenSys, Photometrics, Tucson, AZ, USA).

Centrosome enrichment

Centrosomal fractions were prepared from asynchronous HEK293T and LN-229 cells that were preincubated with 60 ng/ml nocodazole and 1 µg/ml cytochalasin D (Sigma-Aldrich) for 1 h at 37°C. Cell lysis was performed using 1 mM Tris-HCl (0.1% 2-mercaptoethanol, 0.5% Triton X-100; adjusted to pH 8.0) by gently rocking cell culture dishes for 10 min at room temperature. Cell lysates were loaded on a 20% Ficoll (F9378, Sigma-Aldrich) cushion and centrifuged at 20,000 x g for 30 min at 4°C. After centrifugation, several 500 µl fractions were collected from 5 ml above to 2 ml below the interface and examined by Western blot analysis.

Cellular microtubule regrowth assay

LN-18 cells stably expressing GFP-FOCAD or GFP were plated on glass coverslips, incubated with 10 µM nocodazole for 5 h under standard growth conditions to induce microtubule depolymerisation, and washed three times in medium to remove nocodazole. Microtubules were then allowed to re-grow for 5 min at 37°C before cells were fixed with ice-cold methanol and stained with anti-TUBA (dilution 1:2,000) to visualize microtubules. Mean length of microtubules nucleated by centrosomes was determined graphically on z-projections obtained by confocal laser scanning microscopy using ImageJ software (http://imagej.nih.gov/ij/). Per cell line, a total of 100 cells from two independent experiments were evaluated.

Live-cell imaging to track RFP-SLAIN2 trajectories

LN-18 cells stably expressing GFP or GFP-FOCAD were seeded on collagen-coated glass bottom dishes (Ibidi, Martinsried, Germany) and transfected with RFP-SLAIN2 vector. Live-

cell imaging was done using a Nikon microscope (Nikon, Tokyo, Japan) equipped with an Andor/Yokogava Spinning disk X1 and an Andor EMCCD camera (Oxford Instruments, Abingdon, UK). A stage-top incubator was used to keep cells at 37°C, and cells were imaged in CO_2-independent medium (Thermo Fisher Scientific). RFP fluorescence signals in the cytoplasm were acquired with 0.2 s exposure time without delay between frames for about 60 s. To track RFP-SLAIN2 comets, image series were analyzed using the Mosaic ParticleTracker 2D and 3D plugin, v1.6, http://mosaic.mpi-cbg.de/ParticleTracker/ [37] of the ImageJ software. For each of the two cell types, i.e. GFP and GFP-FOCAD expressing LN-18 cells, average RFP-SLAIN2 comet velocity (micrometers per minute) was calculated based on mean values from all RFP-SLAIN2 trajectories detectable for at least 5 frames (1 s) per cell ($n>125$) in a total of 30 cells from three independent experiments.

Flow cytometry of propidium iodide-stained cells

LN-18 and LN-229 cells were fixed in ice-cold 70% ethanol at 4°C for at least 16 h. After resuspending the cell pellets in PBS, 40 µg/ml propidium iodide and 100 µg/ml RNase A (both from Sigma-Aldrich) were added for 30 min at 37°C for DNA staining. Fluorescence intensities were measured using a FACSCanto II flow cytometer (Becton Dickinson, Franklin Lakes, NJ, USA). Data processing was done using the Flowing Software 2 (http://www.uskonaskel.fi/flowingsoftware/).

Cell viability assay in response to PLK1 inhibitor BI 6727 (volasertib)

LN-229 cells (8.0×10^3) were seeded in 96-well plates and cultured over night using normal growth medium. BI 6727 (#18193; Cayman Chemicals, Ann Arbor, MI, USA) was added to a final concentration of 100 nM. After 48 h, the number of viable cells was determined by using the CellTiter 96® AQueous One Solution Cell Proliferation Assay (MTS; Promega, Madison, WI, USA) and recording absorbance at 490 nm with a FLUOstar Omega microplate reader (BMG Labtech, Ortenberg, Germany).

Statistical analysis

OS was calculated from the day of first surgery until death or end of follow-up. Logrank test was used to analyze survival data. Cox regression models were built to assess the association of diminished *FOCAD* copy number with OS. Fisher's exact test was used to test for association of clinical variables. All statistical analyses related to tumors and OS were performed using the IBM SPSS Statistics (version 25) software. Functional, cellular, and biochemical assays were statistically evaluated using the two-tailed Student's t-test; values of $p \leq 0.05$ (*), $p \leq 0.01$ (**), and $p \leq 0.001$ (***) were considered statistically significant.

Results

The frequency of *FOCAD* loss increases with WHO grade in diffuse astrocytic gliomas

We have previously shown *KIAA1797/FOCAD* to be frequently deleted in glioma cell lines and a small series of glioblastomas [4]. Using array-based CGH analysis, we determined *FOCAD* copy number in 133 diffuse astrocytic tumors of WHO grades II to IV, including 36 diffuse astrocytomas, IDH-mutant, WHO grade II, 27 anaplastic astrocytomas, IDH-mutant, WHO grade III, 8 glioblastomas, IDH-mutant, WHO grade IV, and 62 glioblastomas, IDH-wildtype, WHO grade IV. Among the IDH-mutant tumors, diffuse astrocytomas (WHO grade II) rarely demonstrated *FOCAD* loss (in 5.6% of cases), while this alteration was detected in 22.2% of anaplastic astrocytomas (WHO grade III) and 37.5% of glioblastomas (WHO grade IV). Thus, the rate of *FOCAD* loss increased with WHO grade in IDH-mutant diffuse astrocytic gliomas ($p=0.025$), whereas *FOCAD* homozygous deletion was not observed. Of all analyzed tumor entities, a diminished *FOCAD* copy number was most common in IDH-wildtype glioblastomas (51.6%) including *FOCAD* loss in 35.5% and *FOCAD* homozygous deletion in 16.1% of cases (Table 2).

***FOCAD* loss is associated with inferior OS in patients with IDH-mutant astrocytic gliomas**

Next, we explored the potential prognostic role of diminished *FOCAD* copy number in our cohort of 133 patients. *FOCAD* loss was associated with increased risk of death with a HR of 2.6 (95% CI 1.1-6.2) in the group of patients with IDH-mutant tumors (Fig. 1a). In contrast, no association of diminished, i.e. loss or homozygous deletion, versus balanced *FOCAD* copy number with OS was seen in the group of patients with IDH-wildtype glioblastomas (HR=1.1 95% CI 0.6-1.8) (Fig. 1b).

In multivariate analysis of a cohort of 125 patients with available data for all items considering patient age at diagnosis, IDH mutation status, *MGMT* promoter methylation status, and absence or presence of *CDKN2A/B* homozygous deletion, *FOCAD* loss retained significance as a prognostic marker (Table 3). An interaction term for *FOCAD* and IDH status was included and tested (p=0.025). This interaction term emphasized the significant difference in OS for diminished, i.e. loss or homozygous deletion, versus balanced *FOCAD* copy number in patients with IDH-mutant astrocytic gliomas (HR=2.9, 95% CI 1.2-7.1, p=0.023) versus patients with IDH-wildtype glioblastomas (HR=0.8, 95% CI 0.4-1.6, p=0.480) after adjustment for age, *MGMT* promoter methylation status, and *CDKN2A/B* homozygous deletion status.

FOCAD and a C-terminal fragment of tubulin beta-6 (TUBB6) interact in a yeast two-hybrid screen

To explore the molecular basis of the prognostic effect associated with *FOCAD* loss, we screened for FOCAD-interacting proteins using a yeast two-hybrid system. The *S. cerevisiae* strain EGY48 was co-transformed with FOCAD as bait in a LexA fusion pEG202 vector and a human fetal brain cDNA library in a B42-expressing pJG4-5 prey vector. Within the screen, we analyzed specific growth of about 3.5 x 10^6 distinct co-transformants. Prey vectors from the 20 colonies specifically growing on glucose-free galactose/raffinose (SD(gal/raf)ΔHLT) but not on glucose-containing (SD(glu)ΔHLT) plates (Fig. 2a), which are considered to be

true-positive clones, were analyzed by direct DNA sequencing. Thereby, in-frame fragments from three genes were identified, one of which was not followed up because it encodes the C-terminus of a nuclear protein while FOCAD is located in the cytoplasm. The other two sequence fragments encode the C-terminus of heat shock protein 90 alpha family class B member 1 (HSP90AB1; amino acids 641-724) and TUBB6 (amino acids 354-446). Binding of FOCAD to full-length HSP90AB1 was verified by pull-down assay (Suppl. Fig. 1 online resource), whereas the functional relevance of this interaction was not analyzed further. The interaction between FOCAD and the TUBB6-fragment was confirmed by retransforming a fresh yeast EGY48 clone with several combinations of bait vectors, i.e. pEG202-FOCAD, pEG202 empty (negative control), or pEG202-p53 (positive control), and prey vectors, i.e. pJG4-5-TUBB6 (amino acids 354-446), pJG4-5 empty (negative control), or pJG4-5-LTA (positive control). Thereby, yeast growth on SD(gal/raf)ΔHLT selective medium was only observed for FOCAD-TUBB6 (amino acids 354-446) and p53-LTA co-transformants (Fig. 2b). Comparable growth of yeast co-transformants was verified on SD(gal/raf)ΔHT (with leucine) medium (Fig. 2b).

FOCAD binds to several members of tubulin subfamilies, including tubulin gamma-1 (TUBG1)

To verify FOCAD interaction with full-length TUBB6 and to investigate potential binding to other tubulin isoforms of the alpha-, beta-, and gamma-tubulin subfamilies, we performed pull-down assays on lysates of transiently transfected HEK293T cells. Thereby, co-elution of untagged FOCAD from protein-G-sepharose beads was shown after immunoprecipitation (IP) of Myc-TUBB6 using an anti-Myc antibody (Fig. 2c), and after IP of the isoform most homologous to TUBB6, i.e. tubulin beta-3 (TUBB3), which was also Myc-tagged (Fig. 2d). Interestingly, FOCAD co-precipitation was also detected after IP of Myc-TUBG1 (Fig. 2e), whereas binding to Myc-tagged tubulin alpha-1A (TUBA1A) was not observed (Fig. 2f).

FOCAD is enriched at the centrosome in proximity to centrioles

To visualize the cellular site of FOCAD interaction with TUBB6, TUBB3 and tubulin gamma (TUBG), immunofluorescence experiments were performed. By transiently expressing GFP-tagged FOCAD in U-87MG cells carrying a homozygous *FOCAD* deletion (*FOCAD*$^{-/-}$; [4]), co-localization of FOCAD-GFP with overexpressed Myc-TUBB6 and endogenous TUBB3 and TUBG was detected at the centrosome (Fig. 3a, arrows).

To verify the centrosomal and estimate the subcentrosomal localization of FOCAD, co-localization studies with the endogenous centriole-associated proteins centrin (CETN) and SAS-6 centriolar assembly protein (SASS6) in addition to TUBG, primarily localized at the pericentriolar matrix (PCM) surrounding the centrioles, were performed in interphase and mitotic LN-18 cells stably expressing GFP-FOCAD. Using epifluorescence and confocal microscopy, the TUBG signal showing a PCM-like pattern only partially co-localized with the centriolar-shaped GFP-FOCAD signal (Fig. 3b, Suppl. Fig. 2 online resource). Two distinct centrioles were visualized by staining with anti-CETN, and GFP-FOCAD showed a similar staining pattern. Compared to staining of SASS6, which is functionally involved in procentriole formation, GFP-FOCAD signals were more diffuse and also found at other centrosomal loci. Taken together, FOCAD was found in close proximity to centriole pairs in interphase and mitotic cells (Fig. 3b).

To exclude artefacts caused by ectopic expression or by interaction with the GFP-tag, we carried out centrosome enrichment by centrifugation using normal HEK293T cells and LN-229 cells without *FOCAD* deletion [4]. Several fractions of total cell lysates around the phase interface were examined by Western blot analysis. In both cell lines, greatest abundance of endogenous FOCAD was found in those fractions that contained highest levels of TUBG and CETN, which is direct evidence that FOCAD is a centrosomal component (Fig. 3c). Moreover, immunostaining with anti-FOCAD and anti-TUBG antibodies confirmed partial co-localization at the centrosome in human astrocytes expressing endogenous FOCAD [4], but not in LN-18 cells carrying a homozygous *FOCAD* deletion (*FOCAD*$^{-/-}$; [4]) (Suppl. Fig. 3 online resource).

FOCAD is recruited to microtubules via SLAIN motif family member 2 (SLAIN2) and has functional relevance on microtubule dynamics

This study establishes FOCAD as a tubulin-binding protein localizing to centrosomes. Recently, FOCAD was shown to interact with SLAIN2 [16], a key component of the microtubule plus-end tracking protein network [41]. Therefore, we went on to visualize FOCAD and SLAIN2 interactions on a cellular level. After transient overexpression of FOCAD-GFP and RFP-SLAIN2 in HEK293T cells and human astrocytes, both proteins co-localized at interphase and metaphase centrosomes (Fig. 4a, b), at the prometaphase spindle (Fig. 4b), and at microtubules, where FOCAD-GFP was translocated in the presence of RFP-SLAIN2 (Fig. 4a, b, Suppl. Fig. 4 online resource).

To investigate the relevance of FOCAD for microtubule growth and assembly, we analyzed (i) cellular microtubule regrowth after release from the microtubule-depolymerizing agent nocodazole and (ii) microtubule growth velocity / assembly rate measured by RFP-SLAIN2 movement at the growing microtubule plus-ends by live-cell imaging, in LN-18 cells (*FOCAD*$^{-/-}$) stably transfected with GFP-FOCAD or GFP. Mean length of microtubules nucleated by centrosomes 5 min after nocodazole wash out (Fig. 4c), and mean RFP-SLAIN2 comet velocity (Fig. 4d, e) were significantly reduced in LN-18 cells expressing GFP-FOCAD versus GFP. Both experiments demonstrated a functional relevance of FOCAD for microtubule dynamics, indicating significantly slower microtubule growth rates in the presence of FOCAD presumably due to a reduction of SLAIN2 activity at microtubule plus-ends.

FOCAD levels peak in G2/M phase, and stable FOCAD knockdown accelerates progression through G2/M

We have previously shown that FOCAD decreases glioma cell growth *in vitro* and *in vivo* [4]. Here, we explored whether FOCAD impacts cell cycle regulation using a knockdown model of FOCAD expressing LN-229 cells. To monitor FOCAD expression during the cell cycle,

control LN-229 cells stably transduced with a non-targeted shRNA (control shRNA) were synchronized in G1/S or M phase with a double thymidine or nocodazole block procedure. At specific time points after release from these blockades, endogenous FOCAD levels in cell lysates were analyzed by immunoblotting using an anti-FOCAD antibody (Fig. 5a). Histone H3 phosphorylation associated with highly condensed chromatin served as a mitotic marker. FOCAD expression peaked 8-10 h after release from blockade in G1/S phase and 24 h after release from M phase block. Both time points represent G2/M phase as indicated by strongly positive phosphorylation of histone H3 starting around 10 h after release from G1/S and 24 h after release from M phase blockade (Fig. 5a). Similar results were obtained when studying synchronized LN-18 and HeLa S3 cells overexpressing FOCAD-GFP (Suppl. Fig. 5 online resource). Treatment with the 26S proteasome complex inhibitors bortezomib and MG132 suggested regulation of FOCAD protein levels by the ubiquitin proteasome pathway, including the 26S proteasome (Suppl. Fig. 6 online resource), which is involved in cell cycle progression.

Stable FOCAD knockdown (FOCAD shRNA) accelerated progression through the G2/M phase of the cell cycle compared to control shRNA knockdown in LN-229 cells (Fig. 5b-d). This was shown using flow cytometry by measuring DNA content in propidium iodide-stained LN-229 FOCAD knockdown versus control cells. Differences in time-dependent cell cycle progression were most pronounced at 8-10 h after release from G1/S block, i.e. during G2/M phase, when FOCAD expression levels were highest in control cells (Fig. 5a-c). The detected knockdown effect was partially reversed after stable re-expression of FOCAD in knockdown cells (FOCAD shRNA + rescue; Fig. 5b, c). Similarly, accelerated G2/M progression and earlier entry into mitosis in FOCAD knockdown versus control cells reversed by FOCAD re-expression were shown by Western blot analysis of G2/M regulator cyclin B1 expression and mitotic marker histone H3 phosphorylation, in the LN-229 knockdown model (Fig. 5d).

FOCAD influences polo like kinase 1 (PLK1) T210 phosphorylation, and stable FOCAD knockdown increases sensitivity to the PLK1 inhibitor volasertib

Since PLK1 is a key signaling molecule in cell cycle progression with an important role in mitotic entry regulation [28, 38], activating PLK1 T210 phosphorylation was analyzed in the LN-229 FOCAD knockdown model (Fig. 5e, f). Eight hours after release from G1/S block when FOCAD expression was high and the effect of FOCAD knockdown on cell cycle progression and mitotic entry commenced, PLK1 T210 phosphorylation was significantly enhanced in FOCAD knockdown versus control cells (Fig. 5e, f). Therefore, in the LN-229 FOCAD knockdown model we explored whether a PLK1 inhibitor would have an enhanced effect in cells with reduced FOCAD expression. Incubation with the PLK1 inhibitor BI 6727 (volasertib) was found to significantly decrease viability of FOCAD knockdown compared to control cells (Fig. 5g). These data suggest that patients with astrocytic gliomas carrying a *FOCAD* loss might specifically benefit from PLK1 inhibition.

Discussion

Established prognostic factors for OS of patients with diffuse astrocytic gliomas include age at diagnosis as well as IDH mutation and *MGMT* promoter methylation status of the tumor DNA [47]. In the present study, diminished copy number of the *FOCAD* tumor suppressor gene was found to be most common in tumors of the highest malignancy grade (WHO grade IV), in particular in the clinically most aggressive IDH-wildtype glioblastomas, the only examined tumor entity harboring *FOCAD* homozygous deletion in a subset of cases (16.1%). Moreover, we found that *FOCAD* loss was associated with inferior outcome in patients with IDH-mutant diffuse astrocytic gliomas of WHO grades II to IV irrespective of age at diagnosis as well as *MGMT* promoter methylation and *CDKN2A/B* homozygous deletion status. In line with our findings, loss of 9p21.3, where *FOCAD* is located in close proximity to the *CDKN2A/B* tumor suppressor gene locus, has previously been implicated in the pathogenesis and the prognosis of various types of tumors, including gliomas. In a recent

PanCancer and PanSoftware analysis spanning 9,423 tumor exomes across 33 cancer types to catalog driver genes and mutations, the *CDKN2A* deletion at 9p21.3 was the most common putatively actionable alteration in 13% of exomes from all tumors and over 40% of glioblastoma exomes [2]. In IDH-mutant astrocytic gliomas, homozygous *CDKN2A/B* deletions arise during tumor progression and have been associated with shorter OS [1, 22, 39]. However, similar to deletions on 1p and 19q that are chromosomal hallmarks of oligodendroglioma, the 9p deletions harboring the *CDKN2A/B* locus in astrocytic gliomas are frequently large, encompassing a chromosomal subband to an entire chromosomal arm [20, 33, 35, 46]. Therefore, it is likely that the broad 9p deletions target more than one driver gene locus. Accordingly, in an effort to identify potential drivers in large 9p deletions in lower grade gliomas, Roy et al. reported that while *CDKN2A* homozygous deletion was associated with poor OS in The Cancer Genome Atlas (TCGA) and validation cohorts, heterozygous *CDKN2A* loss and absent *CDKN2A* mRNA expression without biallelic *CDKN2A* deletion were not [36]. Furthermore, their results support the notion that the inactivation of several genes, such as *PTPRD* and *PLAA* encoding protein tyrosine phosphatase receptor type D and phospholipase A2 activating protein as well as *MTAP* and *KLHL9* coding for methylthioadenosine phosphorylase and kelch like family member 9, likely causes cumulative haploinsufficiency that contributes to tumor aggressiveness in lower grade gliomas [36]. These authors also describe a significantly reduced *FOCAD* mRNA expression in TCGA lower grade gliomas, in line with evidence from this study that *FOCAD* is a gene on 9p21.3 the loss of which plays a role in the clinical outcome of patients with IDH-mutant astrocytic gliomas.

To support our data suggesting that diminished *FOCAD* copy number is associated with astrocytic glioma aggressiveness, we sought to gain further insights into how FOCAD functions as a tumor suppressor. The finding from a yeast two-hybrid screen that FOCAD interacted with TUBB6 led us to localize FOCAD to the interphase and mitotic centrosome. Several other tumor suppressors, including the APC regulator of WNT signaling pathway [12], BRCA1 [18], checkpoint kinase 1 [23], and tumor protein p53 [8] are known to be

permanently or temporarily associated to the centrosome. Numerical and structural centrosome aberrations are hallmarks of almost all solid tumors including tumors of the brain and have been implicated in their etiology [32, 45] (reviewed in [30]). As the centrosome is the main microtubule-organizing center within mammalian cells involved in regulating a variety of important cellular processes, including cell motility, cell cycle progression, and chromosome segregation (reviewed in [44]), it is quite conceivable that deficiency of a centrosomal protein may promote invasive behavior.

Besides localizing FOCAD to centrosomes, this study provides evidence that FOCAD is recruited to interphase microtubules and mitotic spindles when co-expressed with FOCAD-interacting SLAIN2 [16] and affects microtubule dynamics. These cellular organelles are linked in that centrosomes stabilize the minus ends of microtubules that extend their dynamic plus ends toward the cell periphery. Microtubules play a pivotal role in cell migration, e.g. by regulating lamellipodial protrusion formation and focal adhesion dynamics (reviewed in [14]), and their alterations have been linked to cancer progression (reviewed in [9]). Recently, Osswald and colleagues showed that astrocytic gliomas form ultra-long membrane protrusions, so called tumor microtubes, used as routes for brain invasion and to interconnect over long distances, which contain microtubules [31]. Here, we demonstrated reduced microtubule growth rates and diminished comet velocity of microtubule plus-end binding protein SLAIN2 [41], which promotes cell elongation [3], in the presence of FOCAD. Therefore, in astrocytic gliomas with diminished *FOCAD* copy number showing increased microtubule assembly rates, tumor microtube formation may be enhanced. This molecular mechanism may underlie their proliferative and invasive phenotype that we previously detected *in vitro* and *in vivo* using an orthotopic xenograft mouse model [4]. As we have previously shown that FOCAD localizes to focal adhesions [4], i.e. close contacts with the extracellular matrix the dynamics of which are regulated by microtubules (reviewed in [40]), invasive behavior of glioma cells with diminished *FOCAD* copy number may additionally result from dysregulation of focal adhesions. Moreover, because FOCAD can be recruited to microtubules (this study) and focal adhesions [4], it is tempting to speculate that FOCAD may

be relevant for the control of microtubule-mediated focal adhesion turnover, e.g. by acting as an adaptor protein connecting microtubules and focal adhesions. Such a role in coordinating microtubules at focal adhesions to direct cell migration has recently been described for tumor suppressor APC [19]. Linking *FOCAD* loss to increased microtubule assembly with potential implications for focal adhesions and the formation of tumor microtubes, provides further evidence for a role of *FOCAD* loss in enhanced cell motility and aggressive glioma behavior.

Here, FOCAD protein levels were shown to peak in G2/M phase resulting in accelerated G2/M progression upon FOCAD knockdown, and indicating functional relevance of FOCAD during G2/M phase. Consequently, FOCAD inhibits different phases of the cell cycle compared to G1/S phase inhibitors p15 and p16 encoded by *CDKN2A/B* (reviewed in [25]). Therefore, in astrocytic gliomas with broad 9p deletions encompassing *FOCAD* as well as *CDKN2A/B* the cell cycle is accelerated in G2/M as well as G1/S phase, thereby additively promoting growth and diminishing genomic integrity. Furthermore, our data suggest that FOCAD may interfere in cell cycle regulation via the mitotic protein kinase PLK1. Hyperactivation of PLK1 found in many human tumors including gliomas [11] is broadly associated with progression and poor prognosis, e.g. of glioma patients [7]). Not only did cells with reduced FOCAD expression exhibit an increased PLK1 activity, they also showed an enhanced sensitivity to PLK1 inhibitor BI 6727 (volasertib) compared to control cells. Volasertib has clinical efficacy in a range of malignancies and is currently in phase III development as a potential treatment for patients with acute myeloid leukemia (ClinicalTrials.gov ID: NCT01721876) (reviewed in [15]). However, there is also preclinical evidence for a role of PLK1 inhibition in the treatment of gliomas. In an *in vitro* screen of 160 small molecule kinase inhibitors, a PLK1 inhibitor selectively disrupted proliferation of glioblastoma-derived but not normal neural stem cells [10]. In xenograft mouse models, PLK1 inhibition enhanced temozolomide efficacy in *IDH1*-mutant gliomas [21], and combined volasertib and radiation significantly inhibited growth of glioma stem cells and prolonged median survival compared with radiation treatment alone [13]. According to our data, the use of PLK1 inhibitors may be especially beneficial for patients suffering from astrocytic gliomas

with diminished *FOCAD* copy number, including pleomorphic xanthoastrocytomas that frequently harbor large 9p losses [42].

In conclusion, we demonstrated *FOCAD* loss as a prognostic factor for OS of patients with IDH-mutant astrocytic gliomas. By showing that FOCAD (i) is a tubulin binding protein localizing to centrosomes and recruited to microtubules via interaction with SLAIN2, (ii) diminishes microtubule assembly, and (iii) delays G2/M progression in glioma cells possibly by regulating PLK1 activation, we elucidated FOCAD-dependent molecular mechanisms, which when deregulated due to diminished *FOCAD* copy number may increase biological aggressiveness of diffuse astrocytic gliomas. Prospectively, the identified cellular alterations caused by *FOCAD* loss may guide the development of therapeutic approaches specifically tailored for astrocytic gliomas carrying a *FOCAD* deletion, e.g. PLK1 inhibition.

Acknowledgements The authors wish to thank Alexander Pfeifer, Institute of Pharmacology and Toxicology, University of Bonn Medical Center and University of Bonn, Bonn, Germany for providing the lentivector construct expressing FOCAD-GFP; Erich Nigg, Biozentrum, University of Basel, Switzerland for helpful scientific discussions; Rudolf Bauerfeind, Research Core Unit for Laser Microscopy, Hannover Medical School, Germany for technical support with regard to live-cell imaging experiments; and the Cell Sorting Core Facility, Hannover Medical School, Germany.

Author contributions FB, AC, BH, MiW and RGW designed research; FB, AF, AC, MB, and CMT performed research; MSR, MaW, TP, AvD, GR, and PC contributed materials, patient/tumor data and expertise; FB, AC, BH, and RGW analyzed data and made figures; FB, AC, BH, MiW, and RGW wrote the manuscript; all authors reviewed and revised the manuscript.

Compliance with ethical standards

Statement of human rights The study was approved by the appropriate institutional research ethics committees. All procedures were in accordance with their ethical standards and with the 1964 Helsinki declaration and its later amendments or comparable ethical standards.

Funding FB received a grant from the Hochschulinterne Leistungsförderung (HiLF) program at Hannover Medical School. The German Glioma Network was supported by the German Cancer Aid (Stiftung Deutsche Krebshilfe) from 2004 to 2012 (Grant No. 70-3163-Wi 3).

Conflict of interest GR received research grants from Roche and Merck as well as honoraria for advisory board activities from AbbVie. All other authors report no conflict of interest.

References

1. Aoki K, Nakamura H, Suzuki H, Matsuo K, Kataoka K, Shimamura T, Motomura K, Ohka F, Shiina S, Yamamoto T, Nagata Y, Yoshizato T, Mizoguchi M, Abe T, Momii Y, Muragaki Y, Watanabe R, Ito I, Sanada M, Yajima H, Morita N, Takeuchi I, Miyano S, Wakabayashi T, Ogawa S, Natsume A (2018) Prognostic relevance of genetic alterations in diffuse lower-grade gliomas. Neuro Oncol 20:66-77. https://doi.org/10.1093/neuonc/nox132

2. Bailey MH, Tokheim C, Porta-Pardo E, Sengupta S, Bertrand D, Weerasinghe A, Colaprico A, Wendl MC, Kim J, Reardon B, Kwok-Shing Ng P, Jeong KJ, Cao S, Wang Z, Gao J, Gao Q, Wang F, Liu EM, Mularoni L, Rubio-Perez C, Nagarajan N, Cortés-Ciriano I, Zhou DC, Liang WW, Hess JM, Yellapantula VD, Tamborero D, Gonzalez-Perez A, Suphavilai C, Ko JY, Khurana E, Park PJ, Van Allen EM, Liang H; MC3 Working Group; Cancer Genome Atlas Research Network, Lawrence MS, Godzik A, Lopez-Bigas N, Stuart J, Wheeler D, Getz G, Chen K, Lazar AJ, Mills GB, Karchin R, Ding L (2018) Comprehensive Characterization of Cancer Driver Genes and Mutations. Cell 174:1034-1035. https://doi.org/10.1016/j.cell.2018.07.034

3. Bouchet BP, Noordstra I, van Amersfoort M, Katrukha EA, Ammon YC, Ter Hoeve ND, Hodgson L, Dogterom M, Derksen PW, Akhmanova A (2016) Mesenchymal Cell Invasion Requires Cooperative Regulation of Persistent Microtubule Growth by SLAIN2 and CLASP1. Dev Cell 39:708-723. https://doi.org/10.1016/j.devcel.2016

4. Brockschmidt A, Trost D, Peterziel H, Zimmermann K, Ehrler M, Grassmann H, Pfenning PN, Waha A, Wohlleber D, Brockschmidt FF, Jugold M, Hoischen A, Kalla C, Waha A, Seifert G, Knolle PA, Latz E, Hans VH, Wick W, Pfeifer A, Angel P, Weber RG (2012) KIAA1797/FOCAD encodes a novel focal adhesion protein with tumour suppressor function in gliomas. Brain 135:1027-1041. https://doi.org/10.1093/brain/aws045

5. Cancer Genome Atlas Research Network, Brat DJ, Verhaak RG, Aldape KD, Yung WK, Salama SR et al (2015) Comprehensive, integrative genomic analysis of diffuse lower-grade gliomas. N Engl J Med 372:2481-2498. https://doi.org/10.1056/NEJMoa1402121

6. Ceccarelli M, Barthel FP, Malta TM, Sabedot TS, Salama SR, Murray BA, Morozova O, Newton Y, Radenbaugh A, Pagnotta SM, Anjum S, Wang J, Manyam G, Zoppoli P, Ling S, Rao AA, Grifford M, Cherniack AD, Zhang H, Poisson L, Carlotti CG Jr, Tirapelli DP, Rao A, Mikkelsen T, Lau CC, Yung WK, Rabadan R, Huse J, Brat DJ, Lehman NL,

Barnholtz-Sloan JS, Zheng S, Hess K, Rao G, Meyerson M, Beroukhim R, Cooper L, Akbani R, Wrensch M, Haussler D, Aldape KD, Laird PW, Gutmann DH; TCGA Research Network, Noushmehr H, Iavarone A, Verhaak RG (2016) Molecular Profiling Reveals Biologically Discrete Subsets and Pathways of Progression in Diffuse Glioma. Cell 164:550-563. https://doi.org/10.1016/j.cell.2015.12.028

7. Cheng MW, Wang BC, Weng ZQ, Zhu XW (2012) Clinicopathological significance of Polo-like kinase 1 (PLK1) expression in human malignant glioma. Acta Histochem 114:503-509. https://doi.org/10.1016/j.acthis.2011.09.004

8. Ciciarello M, Mangiacasale R, Casenghi M, Zaira Limongi M, D'Angelo M, Soddu S, Lavia P, Cundari E (2001) p53 displacement from centrosomes and p53-mediated G1 arrest following transient inhibition of the mitotic spindle. J Biol Chem 276:19205-19213. https://doi.org/10.1074/jbc.M009528200

9. Cirillo L, Gotta M, Meraldi P (2017) The Elephant in the Room: The Role of Microtubules in Cancer. Adv Exp Med Biol 1002:93-124. https://doi.org/10.1007/978-3-319-57127-0_5

10. Danovi D, Folarin A, Gogolok S, Ender C, Elbatsh AM, Engström PG, Stricker SH, Gagrica S, Georgian A, Yu D, U KP, Harvey KJ, Ferretti P, Paddison PJ, Preston JE, Abbott NJ, Bertone P, Smith A, Pollard SM (2013) A high-content small molecule screen identifies sensitivity of glioblastoma stem cells to inhibition of polo-like kinase 1. PLoS One 8:e77053. https://doi.org/10.1371/journal.pone.0077053

11. Dietzmann K, Kirches E, von Bossanyi, Jachau K, Mawrin C (2001) Increased human polo-like kinase-1 expression in gliomas. J Neurooncol 53:1-11. https://doi.org/10.1023/A:1011808200978

12. Dikovskaya D, Newton IP, Näthke IS (2004) The adenomatous polyposis coli protein is required for the formation of robust spindles formed in CSF Xenopus extracts. Mol Biol Cell 15:2978-2991. https://doi.org/10.1091/mbc.E03-08-0613

13. Dong J, Park SY, Nguyen N, Ezhilarasan R, Martinez-Ledesma E, Wu S, Henry V, Piao Y, Tiao N, Brunell D, Stephan C, Verhaak R, Sulman E, Balasubramaniyan V, de Groot JF (2018) The polo-like kinase 1 inhibitor volasertib synergistically increases radiation efficacy in glioma stem cells. Oncotarget 9:10497-10509. https://doi.org/10.18632/oncotarget.24041

14. Etienne-Manneville S (2013) Microtubules in cell migration. Annu Rev Cell Dev Biol 29:471-499. https://doi.org/10.1146/annurev-cellbio-101011-155711

15. Gjertsen BT, Schöffski P (2015) Discovery and development of the Polo-like kinase inhibitor volasertib in cancer therapy. Leukemia 29:11-19. https://doi.org/10.1038/leu.2014.222

16. Hein MY, Hubner NC, Poser I, Cox J, Nagaraj N, Toyoda Y, Gak IA, Weisswange I, Mansfeld J, Buchholz F, Hyman AA, Mann M (2015) A human interactome in three quantitative dimensions organized by stoichiometries and abundances. Cell 163:712-723. https://doi.org/10.1016/j.cell.2015.09.053

17. Horpaopan S, Spier I, Zink AM, Altmüller J, Holzapfel S, Laner A, Vogt S, Uhlhaas S, Heilmann S, Stienen D, Pasternack SM, Keppler K, Adam R, Kayser K, Moebus S, Draaken M, Degenhardt F, Engels H, Hofmann A, Nöthen MM, Steinke V, Perez-Bouza A, Herms S, Holinski-Feder E, Fröhlich H, Thiele H, Hoffmann P, Aretz S (2015) Genome-wide CNV analysis in 221 unrelated patients and targeted high-throughput sequencing reveal novel causative candidate genes for colorectal adenomatous polyposis. Int J Cancer 136:E578-E589. https://doi.org/10.1002/ijc.29215

18. Hsu LC, White RL (1998) BRCA1 is associated with the centrosome during mitosis. Proc Natl Acad Sci U S A 95:12983-12988. https://doi.org/10.1073/pnas.95.22.12983

19. Juanes MA, Bouguenina H, Eskin JA, Jaiswal R, Badache A, Goode BL (2017) Adenomatous polyposis coli nucleates actin assembly to drive cell migration and microtubule-induced focal adhesion turnover. J Cell Biol 216:2859-2875. https://doi.org/10.1083/jcb.201702007

20. Körber V, Yang J, Barah P, Wu Y, Stichel D, Gu Z, Fletcher MNC, Jones D, Hentschel B, Lamszus K, Tonn JC, Schackert G, Sabel M, Felsberg J, Zacher A, Kaulich K, Hübschmann D, Herold-Mende C, von Deimling A, Weller M, Radlwimmer B, Schlesner M, Reifenberger G, Höfer T, Lichter P (2019) Evolutionary trajectories of IDH^{WT} glioblastomas reveal a common path of early tumorigenesis instigated years ahead of initial diagnosis. Cancer Cell 35:692-704. https://doi.org/10.1016/j.ccell.2019.02.007

21. Koncar RF, Chu Z, Romick-Rosendale LE, Wells SI, Chan TA, Qi X, Bahassi EM (2017) PLK1 inhibition enhances temozolomide efficacy in IDH1 mutant gliomas. Oncotarget 8:15827-15837. https://doi.org/10.18632/oncotarget.15015

22. Korshunov A, Casalini B, Chavez L, Hielscher T, Sill M, Ryzhova M, Sharma T, Schrimpf D, Stichel D, Capper D, Reuss DE, Sturm D, Absalyamova O, Golanov A, Lambo S, Bewerunge-Hudler M, Lichter P, Herold-Mende C, Wick W, Pfister SM, Kool M, Jones DTW, von Deimling A, Sahm F (2019) Integrated molecular characterization of IDH-mutant glioblastomas. Neuropathol Appl Neurobiol 45:108-118. https://doi.org/10.1111/nan.12523

23. Krämer A, Mailand N, Lukas C, Syljuåsen RG, Wilkinson CJ, Nigg EA, Bartek J, Lukas J (2004) Centrosome-associated Chk1 prevents premature activation of cyclin-B-Cdk1 kinase. Nat Cell Biol 6:884-891. https://doi.org/10.1038/ncb1165

24. Krepischi AC, Achatz MI, Santos EM, Costa SS, Lisboa BC, Brentani H, Santos TM, Gonçalves A, Nóbrega AF, Pearson PL, Vianna-Morgante AM, Carraro DM, Brentani RR, Rosenberg C (2012) Germline DNA copy number variation in familial and early-onset breast cancer. Breast Cancer Res 14:R24. https://doi.org/10.1186/bcr3109

25. LaPak KM, Burd CE (2014) The molecular balancing act of p16(INK4a) in cancer and aging. Mol Cancer Res 12:167-183. https://doi.org/10.1158/1541-7786.MCR-13-0350

26. Louis DN, Ohgaki H, Wiestler OD, Cavenee WK (2007) World Health Organization histological classification of tumours of the central nervous system. International Agency for Research on Cancer, Lyon

27. Louis DN, Ohgaki H, Wiestler OD, Cavenee WK (2016) World Health Organization histological classification of tumours of the central nervous system. International Agency for Research on Cancer, Lyon

28. Macůrek L, Lindqvist A, Lim D, Lampson MA, Klompmaker R, Freire R, Clouin C, Taylor SS, Yaffe MB, Medema RH (2008) Polo-like kinase-1 is activated by aurora A to promote checkpoint recovery. Nature 455:119-123. https://doi.org/10.1038/nature07185

29. Natrajan R, Mackay A, Lambros MB, Weigelt B, Wilkerson PM, Manie E, Grigoriadis A, A'hern R, van der Groep P, Kozarewa I, Popova T, Mariani O, Turajlic S, Furney SJ,

Marais R, Rodruigues DN, Flora AC, Wai P, Pawar V, McDade S, Carroll J, Stoppa-Lyonnet D, Green AR, Ellis IO, Swanton C, van Diest P, Delattre O, Lord CJ, Foulkes WD, Vincent-Salomon A, Ashworth A, Henri Stern M, Reis-Filho JS (2012) A whole-genome massively parallel sequencing analysis of BRCA1 mutant oestrogen receptor-negative and -positive breast cancers. J Pathol 227:29-41. https://doi.org/10.1002/path.4003

30. Nigg EA, Schnerch D, Ganier O (2017) Impact of Centrosome Aberrations on Chromosome Segregation and Tissue Architecture in Cancer. Cold Spring Harb Symp Quant Biol 82:137-144. https://doi.org/10.1101/sqb.2017.82.034421

31. Osswald M, Jung E, Sahm F, Solecki G, Venkataramani V, Blaes J, Weil S, Horstmann H, Wiestler B, Syed M, Huang L, Ratliff M, Karimian Jazi K, Kurz FT, Schmenger T, Lemke D, Gömmel M, Pauli M, Liao Y, Häring P, Pusch S, Herl V, Steinhäuser C, Krunic D, Jarahian M, Miletic H, Berghoff AS, Griesbeck O, Kalamakis G, Garaschuk O, Preusser M, Weiss S, Liu H, Heiland S, Platten M, Huber PE, Kuner T, von Deimling A, Wick W, Winkler F (2015) Brain tumour cells interconnect to a functional and resistant network. Nature 528:93-98. https://doi.org/10.1038/nature16071

32. Pihan GA, Purohit A, Wallace J, Knecht H, Woda B, Quesenberry P, Doxsey SJ (1998) Centrosome defects and genetic instability in malignant tumors. Cancer Res 58:3974-3985

33. Reifenberger G, Weber RG, Riehmer V, Kaulich K, Willscher E, Wirth H, Gietzelt J, Hentschel B, Westphal M, Simon M, Schackert G, Schramm J, Matschke J, Sabel MC, Gramatzki D, Felsberg J, Hartmann C, Steinbach JP, Schlegel U, Wick W, Radlwimmer B, Pietsch T, Tonn JC, von Deimling A, Binder H, Weller M, Loeffler M; German Glioma Network (2014) Molecular characterization of long-term survivors of glioblastoma using genome- and transcriptome-wide profiling. Int J Cancer 135:1822-1831. https://doi.org/10.1002/ijc.28836

34. Reifenberger G, Wirsching HG, Knobbe-Thomsen CB, Weller M (2017) Advances in the molecular genetics of gliomas - implications for classification and therapy. Nat Rev Clin Oncol 14:434-452. https://doi.org/10.1038/nrclinonc.2016.204

35. Riehmer V, Gietzelt J, Beyer U, Hentschel B, Westphal M, Schackert G, Sabel MC, Radlwimmer B, Pietsch T, Reifenberger G, Weller M, Weber RG, Loeffler M; German

Glioma Network (2014) Genomic profiling reveals distinctive molecular relapse patterns in IDH1/2 wild-type glioblastoma. Genes Chromosomes Cancer 53:589-605. https://doi.org/10.1002/gcc.22169

36. Roy DM, Walsh LA, Desrichard A, Huse JT, Wu W, Gao J, Bose P, Lee W, Chan TA (2016) Integrated Genomics for Pinpointing Survival Loci within Arm-Level Somatic Copy Number Alterations. Cancer Cell 29:737-750. https://doi.org/10.1016/j.ccell.2016.03.025

37. Sbalzarini IF, Koumoutsakos P (2005) Feature point tracking and trajectory analysis for video imaging in cell biology. J Struct Biol 151:182-195. https://doi.org/10.1016/j.jsb.2005.06.002

38. Seki A, Coppinger JA, Jang CY, Yates JR, Fang G (2008) Bora and the kinase Aurora a cooperatively activate the kinase Plk1 and control mitotic entry. Science 320:1655-1658. https://doi.org/10.1126/science.1157425

39. Shirahata M, Ono T, Stichel D, Schrimpf D, Reuss DE, Sahm F, Koelsche C, Wefers A, Reinhardt A, Huang K, Sievers P, Shimizu H, Nanjo H, Kobayashi Y, Miyake Y, Suzuki T, Adachi JI, Mishima K, Sasaki A, Nishikawa R, Bewerunge-Hudler M, Ryzhova M, Absalyamova O, Golanov A, Sinn P, Platten M, Jungk C, Winkler F, Wick A, Hänggi D, Unterberg A, Pfister SM, Jones DTW, van den Bent M, Hegi M, French P, Baumert BG, Stupp R, Gorlia T, Weller M, Capper D, Korshunov A, Herold-Mende C, Wick W, Louis DN, von Deimling A (2018) Novel, improved grading system(s) for IDH-mutant astrocytic gliomas. Acta Neuropathol 136:153-166. https://doi.org/10.1007/s00401-018-1849-4

40. Stehbens S, Wittmann T (2012) Targeting and transport: how microtubules control focal adhesion dynamics. J Cell Biol 198:481-489. https://doi.org/10.1083/jcb.201206050

41. van der Vaart B, Manatschal C, Grigoriev I, Olieric V, Gouveia SM, Bjelic S, Demmers J, Vorobjev I, Hoogenraad CC, Steinmetz MO, Akhmanova A (2011) SLAIN2 links microtubule plus end-tracking proteins and controls microtubule growth in interphase. J Cell Biol 193:1083-1099. https://doi.org/10.1083/jcb.201012179

42. Vaubel RA, Caron AA, Yamada S, Decker PA, Eckel Passow JE, Rodriguez FJ, Nageswara Rao AA, Lachance D, Parney I, Jenkins R, Giannini C (2018) Recurrent copy number alterations in low-grade and anaplastic pleomorphic xanthoastrocytoma

with and without BRAF V600E mutation. Brain Pathol. 28:172-182. https://doi.org/10.1111/bpa.12495

43. Venkatachalam R, Verwiel ET, Kamping EJ, Hoenselaar E, Görgens H, Schackert HK, van Krieken JH, Ligtenberg MJ, Hoogerbrugge N, van Kessel AG, Kuiper RP (2011) Identification of candidate predisposing copy number variants in familial and early-onset colorectal cancer patients. Int J Cancer 129:1635-1642. https://doi.org/10.1002/ijc.25821

44. Vertii A, Hehnly H, Doxsey S (2016) The Centrosome, a Multitalented Renaissance Organelle. Cold Spring Harb Perspect Biol 8:a025049. https://doi.org/10.1101/cshperspect.a025049

45. Weber RG, Bridger JM, Benner A, Weisenberger D, Ehemann V, Reifenberger G, Lichter P (1998) Centrosome amplification as a possible mechanism for numerical chromosome aberrations in cerebral primitive neuroectodermal tumors with TP53 mutations. Cytogenet Cell Genet 83:266-269. https://doi.org/10.1159/000015168

46. Weller M, Weber RG, Willscher E, Riehmer V, Hentschel B, Kreuz M, Felsberg J, Beyer U, Löffler-Wirth H, Kaulich K, Steinbach JP, Hartmann C, Gramatzki D, Schramm J, Westphal M, Schackert G, Simon M, Martens T, Boström J, Hagel C, Sabel M, Krex D, Tonn JC, Wick W, Noell S, Schlegel U, Radlwimmer B, Pietsch T, Loeffler M, von Deimling A, Binder H, Reifenberger G (2015) Molecular classification of diffuse cerebral WHO grade II/III gliomas using genome- and transcriptome-wide profiling improves stratification of prognostically distinct patient groups. Acta Neuropathol 129:679-693. https://doi.org/10.1007/s00401-015-1409-0

47. Weller M, van den Bent M, Tonn JC, Stupp R, Preusser M, Cohen-Jonathan-Moyal E, Henriksson R, Le Rhun E, Balana C, Chinot O, Bendszus M, Reijneveld JC, Dhermain F, French P, Marosi C, Watts C, Oberg I, Pilkington G, Baumert BG, Taphoorn MJB, Hegi M, Westphal M, Reifenberger G, Soffietti R, Wick W; European Association for Neuro-Oncology (EANO) Task Force on Gliomas (2017) European Association for Neuro-Oncology (EANO) guideline on the diagnosis and treatment of adult astrocytic and oligodendroglial gliomas. Lancet Oncol 18:e315-e329. https://doi.org/10.1016/S1470-2045(17)30194-8

48. Weren RD, Venkatachalam R, Cazier JB, Farin HF, Kets CM, de Voer RM, Vreede L, Verwiel ET, van Asseldonk M, Kamping EJ, Kiemeney LA, Neveling K, Aben KK,

Carvajal-Carmona L, Nagtegaal ID, Schackert HK, Clevers H, van de Wetering M, Tomlinson IP, Ligtenberg MJ, Hoogerbrugge N, Geurts van Kessel A, Kuiper RP (2015) Germline deletions in the tumour suppressor gene FOCAD are associated with polyposis and colorectal cancer development. J Pathol 236:155-164. https://doi.org/10.1002/path.4520

Table 1. Patient characteristics

	All patients (n=133)
Age at diagnosis (years)	
Median (range)	44 (21-80)
Gender	
Male	87 (65.4%)
Female	46 (34.6%)
Histology	
Diffuse astrocytoma, IDH-mutant, WHO grade II	36 (27.1%)
Anaplastic astrocytoma, IDH-mutant, WHO grade III	27 (20.3%)
Glioblastoma, IDH-mutant, WHO grade IV	8 (6.0%)
Glioblastoma, IDH-wildtype, WHO grade IV	62 (46.6%)
Initial surgery	
Gross total resection	52 (44.1%)
Subtotal resection (50-99%)	40 (33.9%)
Partial resection (<50%)	22 (18.6%)
Biopsy	4 (3.4%)
Not available	15
First-line post-operative therapy	
No therapy	39 (29.3%)
Radiotherapy alone	15 (11.3%)
Chemotherapy alone	4 (3.0%)
Radiotherapy plus chemotherapy	75 (56.4%)
Karnofsky performance score	
90-100	69 (56.6%)
70-80	47 (38.5%)
<70	6 (4.9%)
Not available	11
Death	
No	48 (36.1%)
Yes	85 (63.9%)
***MGMT* promoter methylation status**	
Methylated	89 (67.4%)

Unmethylated	43 (32.6%)
Not available	1
IDH status	
Mutated	71 (53.4%)
Wildtype	62 (46.6%)
***FOCAD* status**	
Loss	33 (24.8%)
Homozygous deletion	10 (7.5%)
Balanced	90 (67.7%)
***CDKN2A/B* status**	
Homozygous deletion	30 (23.8%)
No homozygous deletion	96 (76.2%)
Not available	7

Loss (cut-offs <-0.3 >-1.0); homozygous deletion (cut-off ≤-1.0)

Table 2. Distribution of *FOCAD* copy number status in diffuse astrocytic gliomas according to WHO grade and IDH mutation status

	Astrocytoma WHO grade II n=36	Anaplastic astrocytoma WHO grade III n=27	Glioblastoma WHO grade IV n=70			All tumors WHO grades II-IV n=133		
	IDH-mutant	IDH-mutant	IDH-mutant	IDH-wildtype	Total	IDH-mutant	IDH-wildtype	Total
FOCAD								
Loss	2 (5.6%)	6 (22.2%)	3 (37.5%)	22 (35.5%)	25 (35.7%)	11 (15.5%)	22 (35.5%)	33 (24.8%)
Homo del	-	-	-	10 (16.1%)	10 (14.3%)	-	10 (16.1%)	10 (7.5%)
Balanced	34 (94.4%)	21 (77.8%)	5 (62.5%)	30 (48.4%)	35 (50%)	60 (84.5%)	30 (48.4%)	90 (67.7%)
Total	36 (100%)	27 (100%)	8 (100%)	62 (100%)	70 (100%)	71 (100%)	62 (100%)	133 (100%)

Loss (cut-offs <-0.3 >-1.0); homo del, homozygous deletion (cut-off ≤-1.0)

Table 3. Multivariate analysis for OS of the patient cohort (n=125*), i.e. astrocytomas, IDH-mutant, WHO grade II (n=33), anaplastic astrocytomas, IDH-mutant, WHO grade III (n=24), glioblastomas, IDH-mutant, WHO grade IV (n=8), and glioblastomas, IDH-wildtype, WHO grade IV (n=60)

	HR	95% CI	p-value
FOCAD Loss or homo del vs. balanced (ref)	2.9	(1.2-7.1)	0.023
IDH Wt vs. mut (ref)	5.1	(2.4-10.9)	<0.001
Test for interaction *FOCAD* * IDH status	0.3	(0.1-0.8)	0.025
Age >=45 vs. <45 years (ref)	2.0	(1.0-3.8)	0.037
MGMT promoter Unmethylated vs. methylated (ref)	2.0	(1.2-3.4)	0.013
CDKN2A/B Homo del vs. no homo del (ref)	1.6	(0.8-3.3)	0.192

*Eight patients were excluded from multivariate analysis because the *MGMT* promoter methylation status (n=1) or the CDKN2A/B homozygous deletion status (n=7) were not available

Loss (cut-offs <-0.3 >-1.0); homo del, homozygous deletion (cut-off ≤-1.0)

Figure legends

Fig. 1 Associations of diminished *FOCAD* copy number with OS in a series of 133 patients with IDH-mutant diffuse astrocytomas, anaplastic astrocytomas, glioblastomas or IDH-wildtype glioblastomas. Kaplan-Meier plots showing the association of *FOCAD* loss with inferior outcome in pooled IDH-mutant diffuse astrocytomas, anaplastic astrocytomas and glioblastomas (**a**), while *FOCAD* loss or homozygous deletion were not associated with OS in IDH-wildtype glioblastomas (**b**). *FOCAD* homozygous deletion was not detected in IDH-mutant tumors. AII, diffuse astrocytoma, WHO grade II; AAIII, anaplastic astrocytoma, WHO grade III; GBM, glioblastoma, WHO grade IV; wt, wildtype; mut, mutant; homo del, homozygous deletion (cut-off ≤-1.0); loss (cut-offs <-0.3 >-1.0).

Fig. 2 FOCAD is a tubulin-binding protein. **a** The coding sequence of FOCAD was used as bait and a human brain cDNA library as prey in a yeast two-hybrid screen. The FOCAD-bait protein showed positive interaction with a prey-protein subsequently found to contain a C-terminal fragment of TUBB6 (amino acid sequence 354-446), as indicated by growth of the yeast strain co-expressing both vectors on synthetic defined (SD) medium containing galactose and raffinose (SD(gal/raf)ΔHLT). Specificity of bait and prey interaction was confirmed by growth inhibition of the yeast co-transformants on SD medium containing glucose (SD(glu)ΔHLT) because of glucose-induced suppression of the GAL1 promoter controlling expression of the prey vector. **b** The interaction of FOCAD and the TUBB6-fragment was verified by a retransformation experiment with combinations of several bait and prey vectors. Only yeast co-transformants with FOCAD bait- and TUBB6 prey-vector grew on SD(gal/raf)ΔHLT selective medium, as shown for p53-bait and LTA-prey co-transformants used as positive control. Comparable growth of yeast co-transformants was verified on SD(gal/raf)ΔHT medium required for plasmid selection. **c-f** To test the ability of full-length TUBB6 and further tubulin subfamily members to bind FOCAD, HEK293T cells were transiently transfected with untagged FOCAD and/or one of several Myc-tagged tubulin isoforms. FOCAD was co-purified by immunoprecipitation (IP) using an anti-Myc antibody.

FOCAD was found to bind to full-length Myc-TUBB6 (**c**), to its most closely related isoform, i.e. TUBB3, which was also Myc-tagged (**d**), and to Myc-TUBG1 (**e**), but not to Myc-TUBA1A (**f**). Myc-tagged tubulins were detected using an anti-Myc antibody. †, fragment spanning amino acid residues 354-446; arrowhead, position of the specific tubulin bands; asterisk, heavy chain of the anti-Myc antibody used for IP.

Fig. 3 FOCAD localizes to the centrosome in proximity to centrioles. **a** FOCAD-GFP co-localized with overexpressed Myc-TUBB6, endogenous TUBB3 and TUBG at the centrosome (arrows) in transiently transfected U-87MG cells (*FOCAD*$^{-/-}$). **b** Immunofluorescence co-staining with TUBG, CETN, and SASS6 revealed subcentrosomal localization of GFP-FOCAD close to the centriole pairs (inserts with higher magnification) in stably transfected interphase and mitotic LN-18 cells (*FOCAD*$^{-/-}$). **c** After enriching centrosomes by centrifugation, endogenous FOCAD levels were measured in fractions of HEK293T and LN-229 cell lysates and total cell lysates (TCL). FOCAD levels peaked in the same fractions as the centrosomal marker proteins TUBG and CETN. Scale bar = 2.5 µm (a and b).

Fig. 4 FOCAD is translocated to microtubules via plus-end tracking protein SLAIN2 and reduces microtubule regrowth and SLAIN2 comet velocity. **a** FOCAD-GFP was translocated to microtubules in interphase HEK293T cells co-overexpressing SLAIN2, while its localization was diffusely cytoplasmic and centrosomal in cells expressing FOCAD-GFP only. **b** In addition to co-localizing at centrosomes and microtubules in interphase, FOCAD-GFP and RFP-SLAIN2 co-localized at spindle poles and spindles from prometaphase to anaphase in HEK293T cells transiently overexpressing both proteins. **c** Microtubule (MT) regrowth was significantly reduced in LN-18 cells (*FOCAD*$^{-/-}$) expressing GFP-FOCAD versus GFP. Microtubule regrowth was measured after release from 5 h treatment with 10 µM nocodazole in LN-18 cells (*FOCAD*$^{-/-}$) stably expressing GFP-FOCAD or GFP that were fixed 5 min after nocodazole wash out and stained with anti-TUBA. Microtubule regrowth was quantified by

measuring microtubule length nucleated by centrosomes in 50 cells with stable GFP-FOCAD or GFP expression per experiment (mean ± SD of two independent experiments, representative images of each cell line are shown). **d** Average RFP-SLAIN2 comet velocity was significantly reduced in LN-18 cells (*FOCAD*$^{-/-}$) expressing GFP-FOCAD versus GFP. LN-18 cells (*FOCAD*$^{-/-}$) stably expressing GFP-FOCAD or GFP were transiently transfected with RFP-SLAIN2 and time-lapse confocal microscopy of RFP-SLAIN2 comets was performed for intervals of 60 seconds recording 5 frames per second. The trajectories of RFP-SLAIN2 comets were analyzed using the Mosaic Particletracker 2D and 3D plugin of the ImageJ software. Scatter dot plots show average RFP-SLAIN2 comet velocity (>125 trajectories per cell, mean of 30 cells from three independent experiments per cell line). **e** Measurement of RFP-SLAIN2 comet velocity in LN-18 cells (*FOCAD*$^{-/-}$) stably expressing GFP-FOCAD or GFP. Shown are representative overlays of three successive time-lapse images taken at 4 second intervals, whereby the first, second, and third images were pseudocolored in red, green, and blue, respectively. The boxed regions are shown at higher magnification on the right, and 2-3 representative trajectories of RFP-SLAIN2 comets in each image are marked. *, $p < 0.05$; **, $p \leq 0.01$ (Student's *t* test). Scale bar = 5 µm (a, b, c, and e).

Fig. 5 FOCAD protein levels peak in G2/M phase of the cell cycle, and reduced FOCAD expression accelerates progression through G2/M, enhances PLK1 activating T210 phosphorylation and decreases cell viability upon PLK1 inhibition by BI 6727 (volasertib) in LN-229 cells (*FOCAD*$^{+/+}$) with stable FOCAD or control knockdown. **a** FOCAD levels were determined by Western blot analysis in control LN-229 cells stably transduced with a non-targeted shRNA (control shRNA) at different time points after release from G1/S or M phase blockade by double thymidine or nocodazole treatment. FOCAD levels peaked 8-10 h after release from G1/S and 24 h after release from M phase blockade at the entry to mitosis. Histone H3 phosphorylation at serine 10 (pHH3(S10)) served as a mitotic marker and GAPDH as loading control. **b** Cell cycle progression of LN-229 cells with stable FOCAD

knockdown (FOCAD shRNA), control knockdown (control shRNA), and FOCAD re-expression after FOCAD knockdown (FOCAD shRNA + rescue) stained with propidium iodide was analyzed by flow cytometry at several time points after release from G1/S blockade. In typical examples of DNA content histograms, arrows indicate accelerated cell cycle progression through G2/M phase, i.e. at 8-10 h after release from G1/S block when FOCAD expression was highest in control cells (a), in cells with reduced FOCAD expression compared to control cells, an effect diminished by FOCAD re-expression. **c** Quantification of 2N DNA content histograms shown in (b) showing an acceleration in generating daughter cells with a 2N DNA content in cells with reduced FOCAD expression, which was rescued after FOCAD re-expression (mean ± SD of three independent experiments). Stable FOCAD knockdown was verified by Western blot analysis, vinculin (VCL) served as loading control. **d** Time points of mitotic entry of LN-229 FOCAD shRNA, control shRNA, and FOCAD shRNA + rescue cells after release from G1/S blockade were determined by Western blot analysis of cyclin B1 expression and serine 10 phosphorylation of histone H3 (pHH3(S10)). Earlier mitotic entry was detected in cells with reduced FOCAD expression compared to control cells, an effect reversed by FOCAD re-expression. GAPDH served as loading control. One representative experiment from a total of three experiments is shown. **e, f** FOCAD dependency of activating T210 phosphorylation of the cell cycle and mitotic entry regulator PLK1 were determined in LN-229 FOCAD shRNA, control shRNA, and FOCAD shRNA + rescue cells by Western blot analysis at 8 h after release from G1/S blockade (**e**) when FOCAD expression was high in control cells as shown in (a). Densitometric quantification of Western blot analysis shown in (e) detecting a significantly increased relative PLK1 phosphorylation at T210 in cells with reduced FOCAD expression compared to control cells (mean ± SD of three independent experiments) (**f**). **g** FOCAD-dependent sensitivity to PLK1 inhibitor BI 6727 was evaluated by assaying the viability of LN-229 FOCAD shRNA, control shRNA, and FOCAD shRNA + rescue cells after 48 h of inhibitor incubation time. Cells with reduced FOCAD expression showed a significantly decreased viability after PLK1 inhibition

compared to control cells (mean ± SD of three independent experiments performed in triplicate). *, $p < 0.05$ (Student's *t* test).

Figure 1

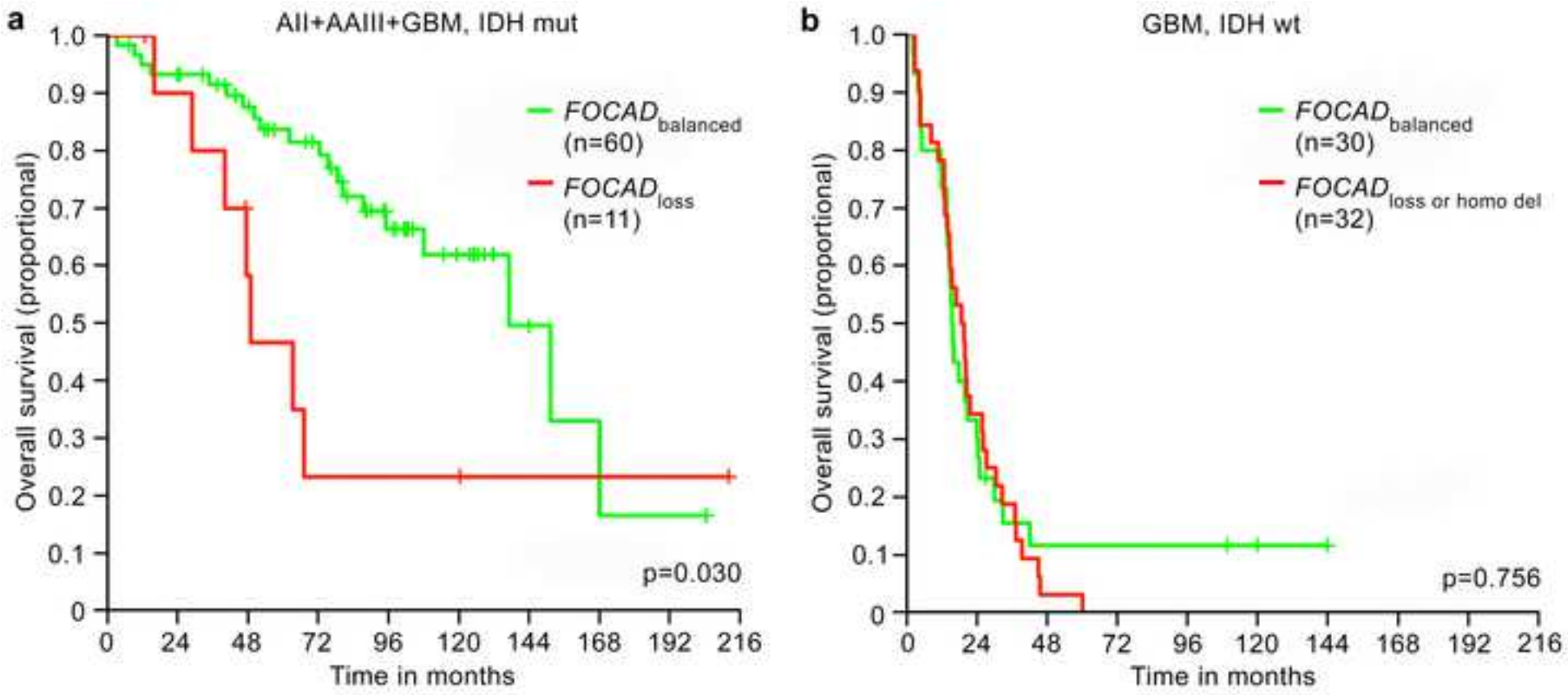

Figure 2

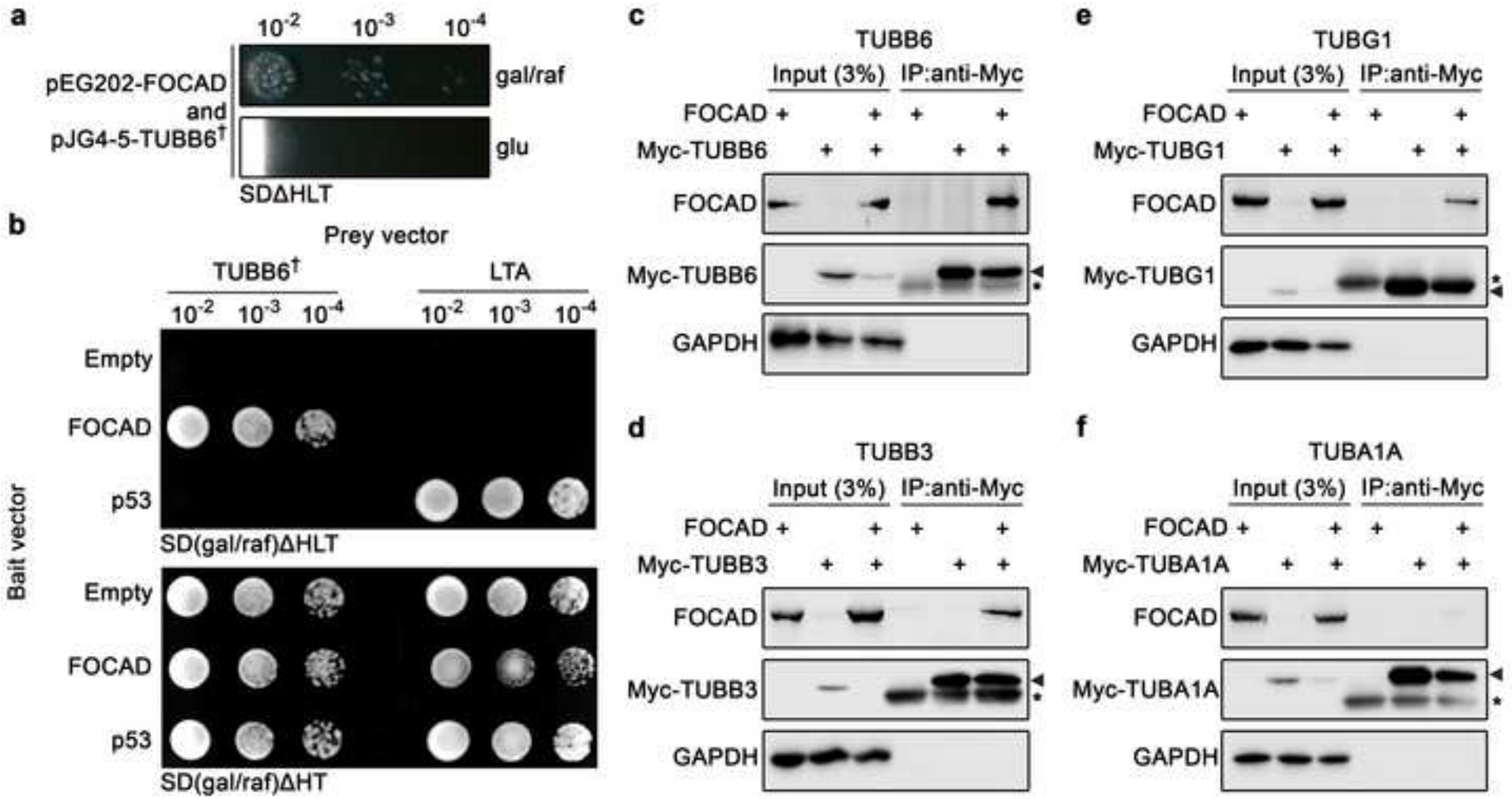

Figure 3

Click here to access/download;figure;Brand et al Figure 3_600dpi.tif

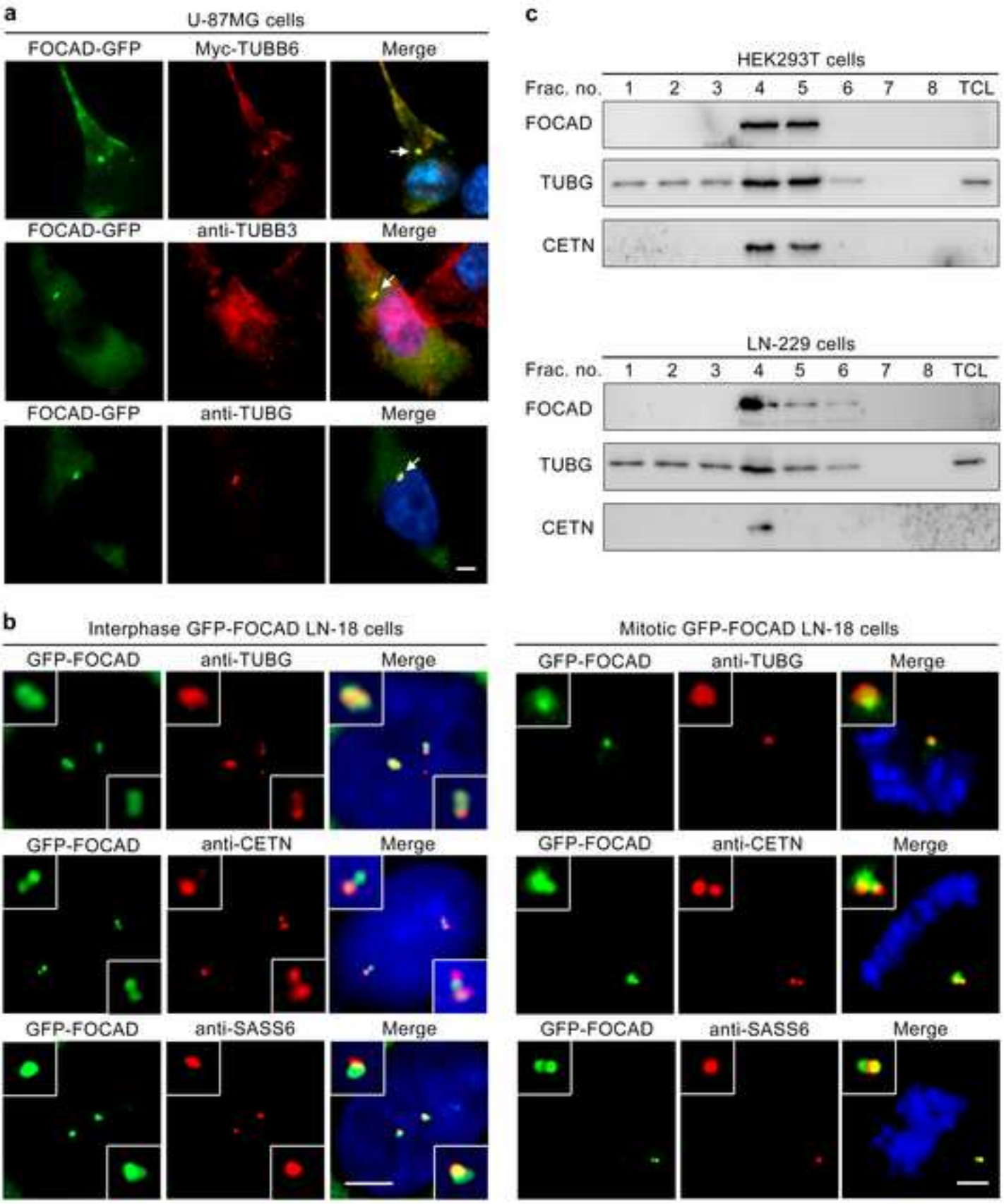

Figure 4

Click here to access/download;figure;Brand et al Figure 4_600dpi.tif

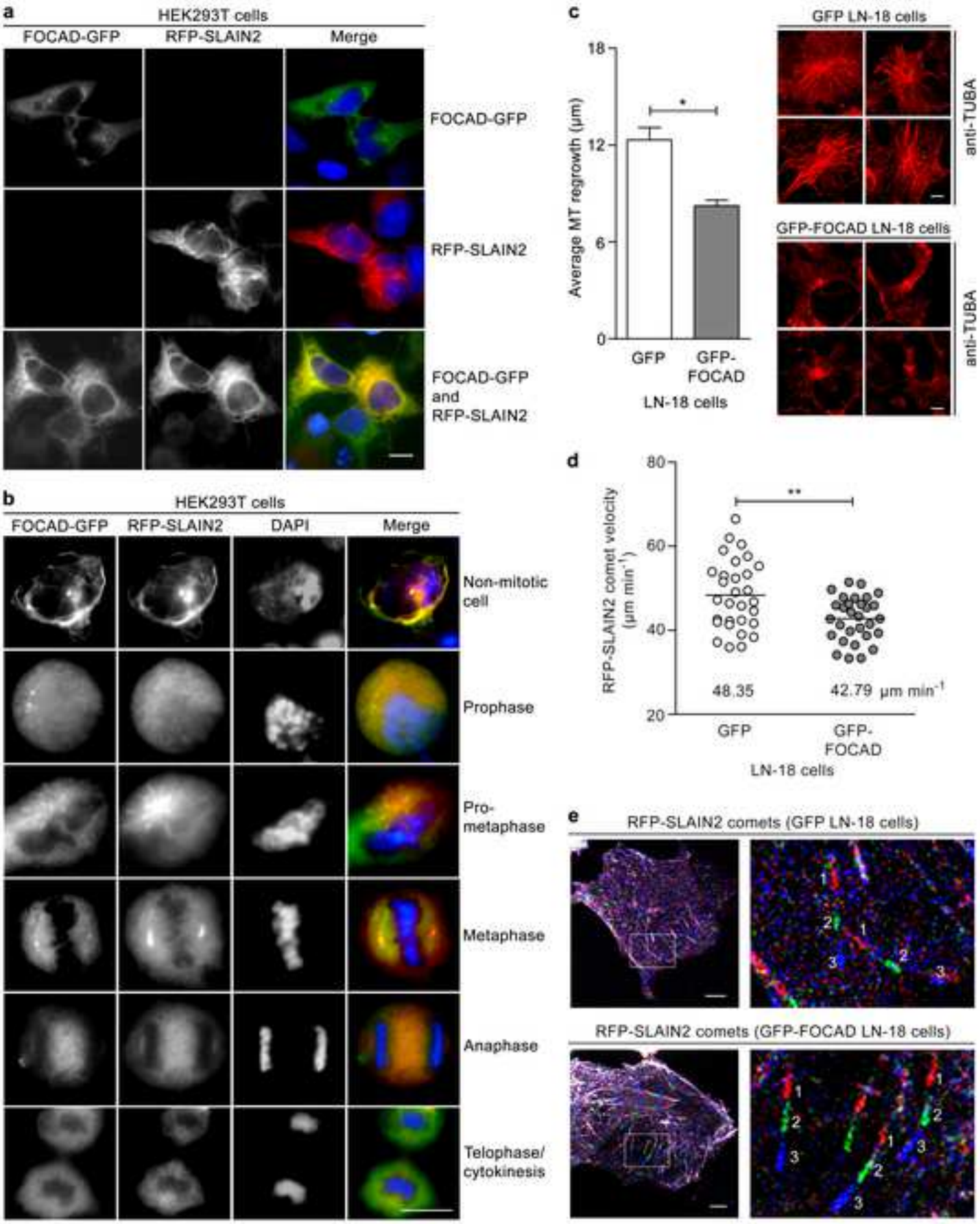

Figure 5

Click here to access/download;figure;Brand et al Figure 5_600dpi.tif